



Rheological kinetics of crosslinking gellan gum— bioactive glass composites

Anastasiia Astanina^{*}, Jonathan Massera^{ID}, Minna Kellomäki^{ID}, Janne T. Koivisto^{ID}

Faculty of Medicine and Health Technology, Tampere University, Korkeakoulunkatu 3, Tampere 33720, Finland

ARTICLE INFO

Keywords:

Hydrogel formulation
Real-time *pH* measurements
Viscoelastic properties
Time sweep
Ultrasonic mixing

ABSTRACT

Gelation kinetics and viscoelastic properties are critical for the biomedical application of hydrogel composites. Specifically, gelation time dictates the injection or processing window. In this study, we aimed to develop mechanically strong, viscoelastic gellan gum-bioactive glass composites by investigating their crosslinking behavior at physiologically relevant *pH* and temperature. We examined how small variations in *pH* and bioactive glass loading influence gelation time, stiffness, and elasticity. Using strain-controlled rheology, we found that gelation occurred from 7.5 to 28 min for composites containing 20–30 wt% glass, demonstrating their suitability for injection and 3D printing. Rheological characterization further confirmed an elastically dominant behavior ($G' > G''$) at all conditions. The strongest crosslinking was observed at 20 wt% glass loading (at *pH* 6.5 and 6.8) and 30 wt% glass loading (at *pH* 7.0). Increasing the glass loading and *pH* broadened the viscoelastic region and shifted the G'/G'' crossover point to higher strains. A key finding of this study was the observed strong influence of small *pH* changes within the range of 6.5–7.0 to the gelation kinetics of the gellan gum-bioactive glass composites.

1. Introduction

Over the past few years, extensive research has been conducted to investigate the gelation kinetics and crosslinking of hydrogels for biomedical applications. The primary goal has been to enhance materials design through a deeper understanding of the factors influencing gelation processes [1–3]. Although several studies have investigated the rheological behavior of hydrogels under various conditions [4–7], they typically do not examine real-time changes in *pH* and temperature during the actual crosslinking process or connect these dynamic parameters to hydrogel network formation. Most studies assess *pH* and temperature as fixed initial conditions rather than continuously monitored parameters during gelation.

Tanaka *et al.* defined gelation time as “the time it takes for the network-forming solution of functional molecules to reach their gel points after the crosslinking reaction begins” [8]. Similarly, Jain *et al.* described gelation time as the point when “the gel precursor stops flowing upon inversion due to gravity, indicating that a solid gel network has formed” [2]. Rheology is a useful method for measuring crosslinking rates. In this study we used rheological kinetics

(rheokinetics) – an approach that tracks changes in viscoelastic properties over time – to analyze the rate of polymerization or crosslinking reactions. Duarte *et al.* introduced the term “rheokinetics” to describe changes in viscoelastic properties over time, enabling kinetic analysis of gelation in polymer mixtures [5]. Several studies have reported the rheological behavior and structure–property relationships of hydrogels, focusing on the behavior under various conditions [4–7]. One of the studied polysaccharides for hydrogels is gellan gum (GG), an exopolysaccharide derived from *Sphingomonas* group. It is a promising biomedical hydrogel matrix due to its biocompatibility. Its repeating unit contains L-rhamnose, D-glucuronic acid, and two D-glucose residues [9]. Similar to other polysaccharides, GG undergoes physical crosslinking by divalent ions, leading to irreversible gelation [10–14]. The gelation time of GG is influenced by *pH*, temperature and the concentration of crosslinking ions [14]. *pH* affects the availability of carboxyl groups (-COOH) for crosslinking, while cooling from elevated temperature induces a coil–helix transition in the GG molecules [15]. This structural change decreases the distance between crosslinking sites. As a result, the crosslinking density increases, leading to mechanically stronger hydrogels [15]. Gering *et al.* assessed the gelation behavior of

^{*} Corresponding author.

E-mail addresses: anastasia.astanina@tuni.fi (A. Astanina), jonathan.massera@tuni.fi (J. Massera), minna.kellomaki@tuni.fi (M. Kellomäki), janne.t.koivisto@tuni.fi (J.T. Koivisto).

<https://doi.org/10.1016/j.mtcomm.2025.114133>

Received 19 August 2025; Received in revised form 18 October 2025; Accepted 20 October 2025

Available online 22 October 2025

2352-4928/© 2025 The Authors. Published by Elsevier Ltd. This is an open access article under the CC BY license (<http://creativecommons.org/licenses/by/4.0/>).

gellan gum (GG)-based hydrogel formulations for various application techniques [7]. In addition, Jongprasitkul *et al.* utilized *in situ* photo-rheology to evaluate the gelation kinetics of Ca^{2+} -crosslinked methacrylated GG at 1 w/v%, 2 w/v%, and 3 w/v% following UV light exposure [16].

Divalent and higher cations are initiating crosslinking of GG; for example, ionic (ionotropic) crosslinking occurs between the negatively charged carboxylate anions of D-glucuronic acid in GG and the positively charged Ca^{2+} and Mg^{2+} ions from salts. Therefore, it is a natural assumption to investigate how effectively ion-release of bioactive glasses (BAG) can facilitate crosslinking [15–18]. Moreover, borosilicate BAG, 13–93B20 is known for its osteostimulative and osteoconductive properties. It is primarily used for hard tissue reconstruction, but it also demonstrates potential benefits when incorporated into hydrogel matrices [19–22]. The borosilicate 13–93B20 BAG combines the congruent dissolution of the borate phase with the non-congruent dissolution of the silicate network. Moreover, borosilicate BAG are shown to degrade faster and more completely than traditional silicate BAGs [23,24].

In our composite, we use 1393-B20 as a ceramic filler. The addition of BAG to GG enhances the mechanical strength of the composite, inhibits enzymatic and hydrolytic degradation, and promotes bioactivity [10]. Vuornos *et al.* found that ions released from BAG improved mechanical properties of GG–spermidine and collagen 3D hydrogels [10]. Douglas *et al.* used stress-controlled rheology to assess the gelation behavior of GG-based hydrogel composites reinforced with various BAGs [17]. They reported that BAG-free samples initially exhibited significantly lower storage modulus (G') compared to BAG-containing samples. However, the overall gelation patterns were similar [17]. In general, incorporating BAG into hydrogel matrix regulates gelation behavior, rheological characteristics, and mechanical properties. Specifically, the addition of BAG particles reduces gelation time by increasing viscosity. Smaller particles dissolve and release ions more rapidly, which enhances crosslinking and particle integration within the hydrogel matrix [10,17,25].

In the current work, we use a fabrication temperature of 23 °C. This temperature is more suitable for biomedical use than the 55 °C used previously [18]. The lower temperature is expected to alter the coil-helix transition dynamics in GG molecules, thus influencing the crosslinking process [15]. As pH increases toward neutral, carboxylic acid groups deprotonate to carboxylate anions, increasing the negative charge density along the polymer chains. This strengthens intra- and interchain electrostatic repulsion due to increased a polyelectrolyte effect and thus its prolongs gelation time [26].

In this study, we focus on showing the effects of pH and glass loading on the rheological kinetics of gelation and viscoelastic properties of GG/BAG composites while producing them at room temperature (23 °C). We hypothesize that even minor pH close to neutral range will affect the number of crosslinks and the speed of gelation, without significantly affecting the rate of BAG dissolution. We aim to understand the crosslinking behavior of GG/BAG when processed at biologically relevant temperatures. Additionally, we monitor the gelation by tracking real-time changes in pH and temperature during crosslinking. Furthermore, we explore how stiffness and elasticity of the final hydrogel composites are affected by slight pH variations near the neutral range in HEPES/Sucrose buffer (termed initial pH), along with variation of glass loading percentage. The observed gelation behavior can be utilized for injectability and printability protocols.

2. Materials and methods

2.1. Materials

GG (Sigma Aldrich, St. Louis, the U.S.A., Lot # SLCC3380) was prepared by dissolution in a HEPES (Sigma Aldrich, St. Louis, the U.S.A., CAS-No: 7365–45–9) / Sucrose (Sigma Aldrich, St. Louis, the U.S.A.,

CAS-No: 57–50–1) buffer (25 mM HEPES / 10 % w/w Sucrose), at 70 °C with a GG concentration of 5 mg ml⁻¹, as described in our previous work [18]. The pH of HEPES / Sucrose buffer was adjusted to 6.5, 6.8, or 7.0 using 1 M NaOH (Fig. 1, Step 1). These starting pH levels of HEPES/Sucrose solution as prepared in the beginning of sample fabrication are referred to as initial pH . The borosilicate BAG used in this work was 13–93B20 (composition in mol%: 43.7SiO₂-10.9B₂O₃-22.1CaO-7.9K₂O-7.7MgO-6.0Na₂O-1.7P₂O₅), prepared as described by Houaoui *et al.* [27]. The glass was produced by melting at 1450 °C, annealing and crushing. Size of the glass microparticles was less than 38 μm. The glass was washed with acetone and dried to remove the smallest microparticles as in the work of Siekkinen *et al.* [28]. The weight ratios between GG and BAG were varied subsequently as follows: 90:10, 80:20, 70:30, 60:40, and 50:50 wt%.

2.2. Preparation stage

The Preparation stage (composed of Step 1 “Mixing of GG” and Step 2 “Addition of BAG”) is illustrated in Fig. 1. The fabrication of composite hydrogels was performed at a temperature of 23.0 ± 0.6 °C. In the first step, GG was mixed with a magnetic stirrer (250 rpm) for 10 min (Fig. 1, Step 1), followed by the addition of BAG microparticles. Subsequently, the GG/BAG mixture was sonicated using an ultrasonic homogenizer (200 W and 26 kHz, Hielscher UP200St, Sonotrode S26d7) for 20 s to improve glass particle dispersion within the hydrogel matrix in the second step (Fig. 1, Step 2). The temperature of the system was increased to 32.2 ± 0.9 °C.

2.3. Gelation stage

The Gelation stage (composed of Step 3 “Mixing of GG/BAG”, Step 4 “Gelation assessment of GG/BAG” and Step 5 “Assessment of fully gelled GG/BAG”) is illustrated in Fig. 1.

2.3.1. Tube tilt test

Gelation time for 5 parallel samples was measured for 10, 20, 30, 40, and 50 wt% glass loadings, at pH 6.5, 6.8, and 7.0, by tube tilt test. The pH and temperature (°C) of GG/BAG were measured with an Orion Star A111 benchtop pH meter (Thermo Fisher Scientific Inc., the U.S.A.). The pH and temperature (°C) of GG/BAG were separately recorded in Steps 1 and 2 (Fig. 1, Step 1–Step 2), while these characteristics were continuously monitored from the third to the final step (Fig. 1, Step 3–Step 5) for 3 parallel samples. In Step 3, after the sonication the GG/BAG mixture was further mixed using a magnetic stirrer for an additional 10 min, and the gelation time recording was started (Fig. 1, Step 3). In Step 4, 650 μl of GG/BAG mixture was poured into a cut-off syringe mold. The mold was then tilted every 30 s for the first 5 min, followed by tilting every 1 min until 30 min had elapsed or gelation occurred (Fig. 1, Step 4). After 30 min, the tilting frequency was reduced to once every 5 min until visual gelation was observed. Once gelation was completed and the sample was no longer flowed when tilted, the time was recorded as the gelation time via the tube tilt test (Fig. 1, Step 5). Real-time pH and temperature were measured from Step 1 to Step 5-initially after 30 s and then with 1-minute intervals for the first 20 min. If gelation time exceeded 20 min, measurements were recorded every 5 min until complete gelation occurred. The temperature during gelation was measured to decrease to 25.1 ± 0.6 °C.

2.3.2. Time sweep

Hydrogel precursor solution was prepared (Fig. 1, Step 1–2) and time sweeps were conducted for 3 parallel samples (Fig. 1, Step 3–Step 5). The measurement was carried out on samples with 10, 20, and 30 wt% glass loadings using a Discovery HR-2 rotational rheometer and TRIOS software (TA Instruments, U.S.A.) at constant strain within a period from 60 to 90 min, depending on the tube tilt results. The setup utilized 20 mm stainless steel plate-plate geometry. Additionally, a solvent trap

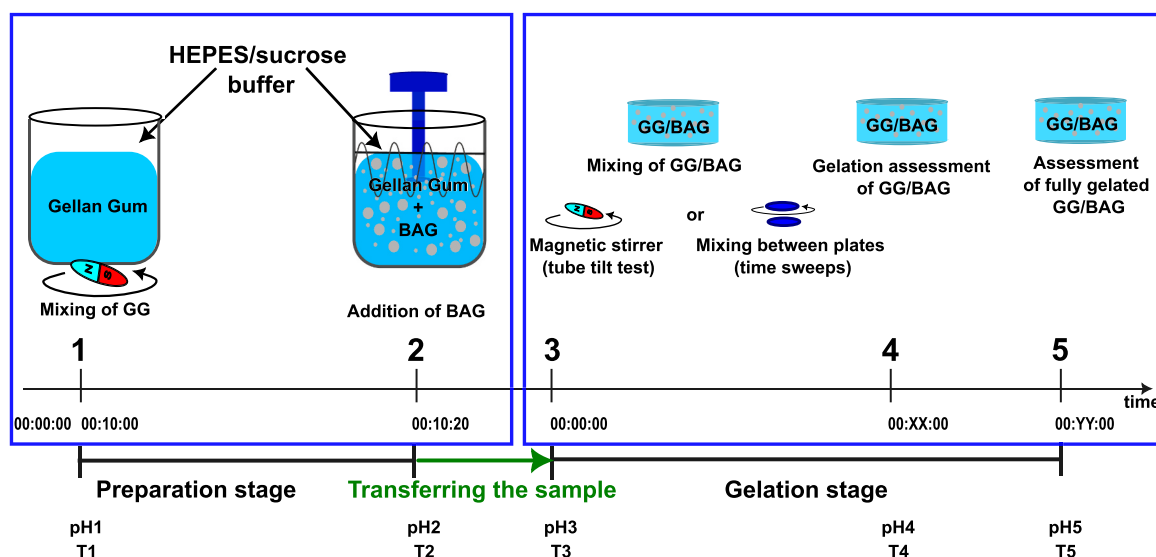


Fig. 1. Fabrication process diagram: Preparation and Gelation stages of GG/BAG composite hydrogels with timeline shown. The transfer of the hydrogel precursor occurred between Step 2 and Step 3 (at tube tilt test: pipetting to the cut-off syringe mold; at time sweep: transferring to rheology geometry). Amplitude and frequency sweeps were implemented after Step 5 when gelation was complete.

was used to impede evaporation. Samples with 40 and 50 wt% glass loadings were excluded from further experiments based on the tube tilt tests due to excessively long gelation times.

After Step 2, 550 μL of GG/BAG was transferred to the rheometer geometry by pipetting between parallel plates with a geometry gap of $1500 \pm 250 \mu\text{m}$ at 23°C . The geometry gap was adjusted manually to reach full contact between the surface of the sample and the plates. Then, in Step 3, an angular frequency of 10.00 rad s^{-1} (frequency 1.59 Hz) at 1.00% strain was applied for 2, 7, or 10 min (Fig. 1, Step 3). Initially, samples were mixed for 10 min, but if gelation occurred too rapidly, the mixing time was gradually decreased to 7, 5, or 2 min as an iterative process.

In Step 4, we evaluated the storage and loss moduli of the material as a function of time, for up to 60–90 min, depending on the sample (Fig. 1, Step 4). In Step 5, complete gelation occurred (Fig. 1, Step 5), and the gelation time was identified as a plateau in the storage modulus curve, indicating the point when the highest storage modulus value was observed, suggesting that GG was fully crosslinked by BAG ions.

2.4. Viscoelasticity of fully crosslinked samples (final stage)

The viscoelastic properties of GG/BAG were monitored by amplitude and frequency sweeps for 3 parallel samples at 23°C using the same rotational rheometer as described above. Samples were prepared using the same gelation procedure as for the tube tilt test and then stored overnight in a humidity chamber at room temperature following Step 5. Initial amplitude sweeps for GG/BAG ranged from 0.01% to 100% oscillation strain at a constant angular frequency of 10.00 rad s^{-1} (equivalent to a frequency of 1.59 Hz) to identify the linear viscoelastic region (LVER) and the oscillation strain at G'/G'' crossover point. After conducting amplitude sweep measurements on 3 parallel samples, the median strain of LVER was used for frequency sweeps. Frequency sweeps were then performed in triplicate, resulting in the recording of the storage (G') and loss (G'') moduli of GG/BAG at frequencies from 0.01 to 10 Hz.

3. Results

3.1. Gelation time from tube tilt test, and real-time pH and temperature (T , $^\circ\text{C}$) monitoring

Gelation times measured from the tube tilt test are summarized in Table S1 for samples with all glass loadings. The gelation process occurred in less than 10 min for samples with 40 and 50 wt% glass loading. This was too rapid to reliably perform tests other than tube tilt test; therefore, only the samples containing 10, 20 and 30 wt% BAG were chosen for further studies.

Gelation times measured from the tube tilt test are summarized in Table S1 for samples with all glass loadings. Table 1 presents pH and temperature at each fabrication step, while Fig. 2 and Table S2 provide real-time monitoring data for these parameters during gelation of 10–30 wt% BAG samples. In general, gelation time decreased with increasing BAG loading, and increased with rising initial pH (from 6.5 to 7.0). Real-time temperature monitoring revealed dynamic changes throughout the gelation process. All samples, regardless of their initial pH, exhibited a temperature rise after BAG addition (T_2), due to ultrasonication, at preparation phase (Step 2). Moreover, nearly all - except those with 30 wt% BAG samples at initial pH 6.5 - showed further increases (T_3 – T_5) during the gelation phase (Steps 3–5). Interestingly, the final temperature of fully gelled GG/BAG samples (T_5) decreased as BAG content increased (Step 5), as shown in Fig. 2 and Table 1. pH was found to increase immediately after BAG was introduced into GG due to the BAG dissolution [19]. This change followed a non-linear pattern: an initial sharp increase during mixing was followed by a slower rise and eventual stabilization until the end of gelation. The speed of pH increase depended on both the initial pH and BAG loading, with higher values leading to a more rapid shift in pH. The zoomed-in figures (Fig. 2E and D), at 20 and 30 wt% of BAG, illustrated this sharp initial pH rise.

3.2. Gelation time from rheology time sweeps

Time sweep rheology confirmed that gelation time increased with higher initial pH and generally decreased with increasing BAG loading. However, at 30 wt% BAG gelation times remained similar across all initial pH values, as shown in the rheological time sweep (Fig. 3), and in the variability of gelation times (Fig. 4). Due to rapid gelation observed after 10 min of mixing, mixing times were reduced: to 7 min for 20 wt%

Table 1

pH and temperature (*T*, °C) measurements in GG/BAG at each fabrication step during the tube tilt test. Increases in temperature during Step 2 and Step 5 are highlighted in bold. For each condition, *n* = 3; values are reported as mean ± standard deviation.

Stage	Preparation stage		Gelation stage		
Step	1. Mixing of GG	2. Addition of BAG	3. Mixing of GG/BAG	4. Gelation assessment of GG/BAG	5. Assessment of fully gelated GG/BAG
BAG, wt%	<i>pH</i> ₁	<i>pH</i> ₂	<i>pH</i> ₃	<i>pH</i> ₄	<i>pH</i> ₅
	<i>T</i> ₁	<i>T</i> ₂	<i>T</i> ₃	<i>T</i> ₄	<i>T</i> ₅
Initial <i>pH</i> (HEPES/Sucrose buffer) = 6.49 at 22.8 °C ¹					
10	6.50±0.04	6.55±0.04	6.84±0.07	6.92±0.09	7.06±0.07
	22.7±0.7 °C	29.2±0.7 °C	22.1±0.5 °C	23.0±0.6 °C	25.5±0.5 °C
20	6.51±0.04	6.74±0.03	7.22±0.05	7.24±0.04	7.27±0.06
	23.0±1.0 °C	32.0±0.9 °C	24.4±0.6 °C	24.6±0.7 °C	24.6±0.5 °C
30	6.49±0.03	6.78±0.09	7.27±0.09	7.30±0.08	7.32±0.08
	23.4±0.9 °C	33.3±0.5 °C	23.1±0.5 °C	23.1±0.5 °C	23.1±0.5 °C
Initial <i>pH</i> (HEPES/Sucrose buffer) = 6.81 at 23.1 °C ²					
10	6.80±0.02	6.83±0.04	7.02±0.02	7.02±0.02	7.19±0.05
	22.7±0.5 °C	36.0±0.9 °C	22.8±0.5 °C	22.8±0.5 °C	25.2±0.9 °C
20	6.82±0.02	6.86±0.02	7.20±0.05	7.23±0.04	7.34±0.03
	23.0±0.5 °C	33.1±0.9 °C	22.6±1.5 °C	22.7±1.5 °C	24.2±0.5 °C
30	6.81±0.01	6.93±0.03	7.41±0.07	7.42±0.07	7.44±0.07
	22.7±0.5 °C	34.9±1.6 °C	22.7±0.9 °C	22.7±0.9 °C	23.1±0.9 °C
Initial <i>pH</i> (HEPES/Sucrose buffer) = 7.01 at 22.9 °C ³					
10	7.00±0.02	7.02±0.02	7.12±0.04	7.13±0.04	7.22±0.09
	23.1±0.5 °C	28.8±0.7 °C	23.5±0.5 °C	23.5±0.5 °C	28.2±0.5 °C
20	7.01±0.02	7.05±0.02	7.38±0.09	7.40±0.09	7.51±0.09
	23.0±0.5 °C	32.7±1.7 °C	23.6±0.5 °C	23.4±0.5 °C	26.8±0.5 °C
30	7.01±0.02	7.05±0.02	7.50±0.03	7.53±0.04	7.63±0.06
	23.0±0.5 °C	30.1±0.5 °C	23.3±0.9 °C	23.4±0.8 °C	25.1±0.5 °C

¹Named as initial *pH* 6.5 in the results.²Named as initial *pH* 6.8 in the results.³Named as initial *pH* 7.0 in the results.

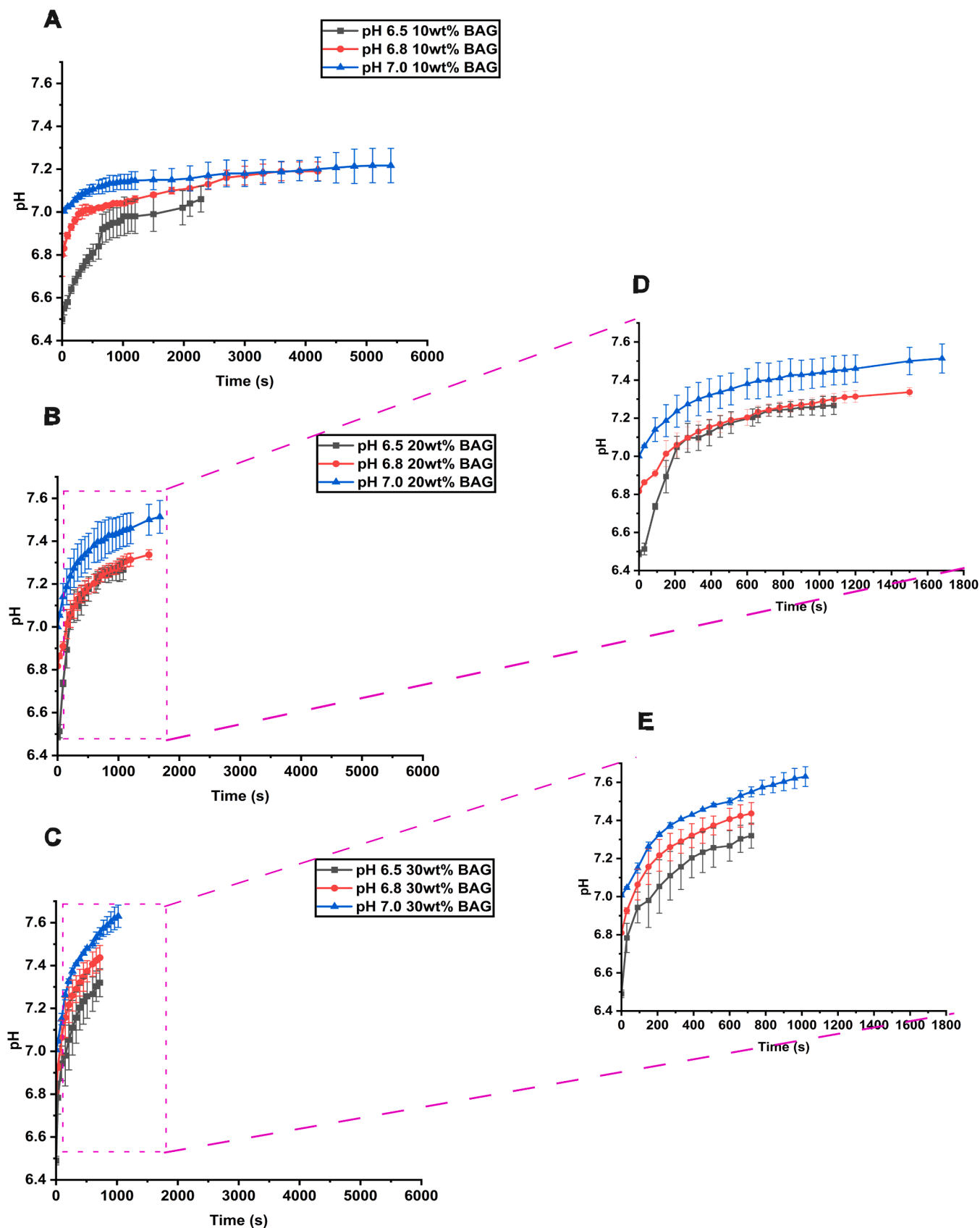


Fig. 2. Real-time pH monitoring during gelation of GG/BAG, in tube tilt test, at the following BAG loadings: A) 10 wt%; B) 20 wt% (zoomed in on D); C) 30 wt% (zoomed in on E). The duration of pH measurements is based on measured gelation time. At each time point n = 3 and values are given as average ± standard deviation.

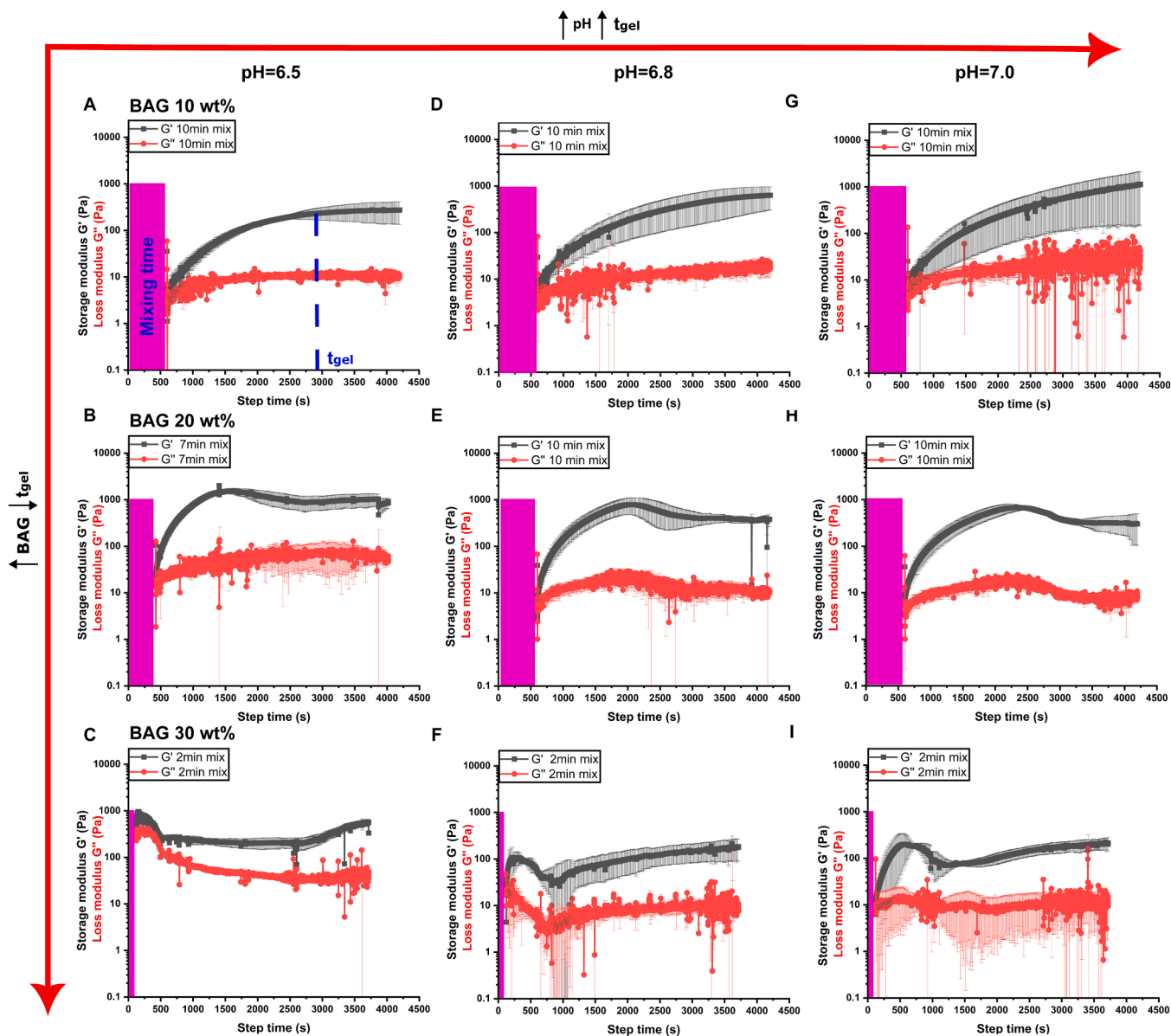


Fig. 3. Strain-controlled time sweep measurements of GG/BAG composites at various pH , glass loadings, and mixing time. pH 6.5 (left column): **A)** 10 wt% BAG (10 min mixing), **B)** 20 wt% BAG (7 min mixing), **C)** 30 wt% BAG (2 min mixing); pH 6.8 (central column): **D)** 10 wt% BAG (10 min mixing), **E)** 20 wt% BAG (10 min mixing), **F)** 30 wt% BAG (2 min mixing); pH 7.0 (right column): **G)** 10 wt% BAG (10 min mixing), **H)** 20 wt% BAG (10 min mixing), **I)** 30 wt% BAG (2 min mixing). An example of recorded gelation time (t_{gel}) is illustrated in A), where G' reaches a plateau. Mixing time is illustrated with a colored box at the beginning of each graph. Due to the fast gelation observed after 10 min of mixing, the mixing time was shortened to 7 min for 20 wt% BAG samples at pH 6.5 and to 2 min for all 30 wt% BAG samples. At each time point $n = 3$ and values are given as average \pm standard deviation.

BAG samples at pH 6.5 and to 2 min for 30 wt% BAG samples at all initial pH values. It was observed that the gelation of 10 wt% BAG samples at pH 6.8 and pH 7.0 occurred overnight, as determined by tube tilt test measurements. Additionally, it was noted that all GG/BAG samples showed high standard deviations in G'' during time sweeps (Fig. 3). This variation is attributed to the presence of glass microparticles in the composite gels, which create regions with varying rigidity in the composite gel structure, leading to differences in viscous response and an increase in the standard deviation in G'' curves.

3.3. Amplitude sweep

Amplitude sweep results (Table 2, Fig. 5) demonstrated that both linear viscoelastic region (LVER) and the strain at the G'/G'' crossover point increased with BAG loading. Changes in initial pH from 6.5 to 7.0

demonstrated changes in LVER and oscillation strain for samples with 10 wt% glass loading, while these values remained similar for samples with 20 and 30 wt% glass loading. In all samples, G'' increased after the LVER before declining past the crossover point. This behavior reflects the structural characteristics of GG/BAG hydrogels: in an aqueous solution at room temperature, the GG backbone is disordered but extended due to the electrostatic repulsion. As a result, molecular arrangement and hydrogen bonding then promote the formation of a weak, structured secondary network [29,30].

3.4. Frequency sweep

The results of the frequency sweep analysis are summarized in Table 2 and illustrated in Fig. 6. All frequency sweep tests demonstrated that G' was higher than G'' , indicating that the material has a dominant

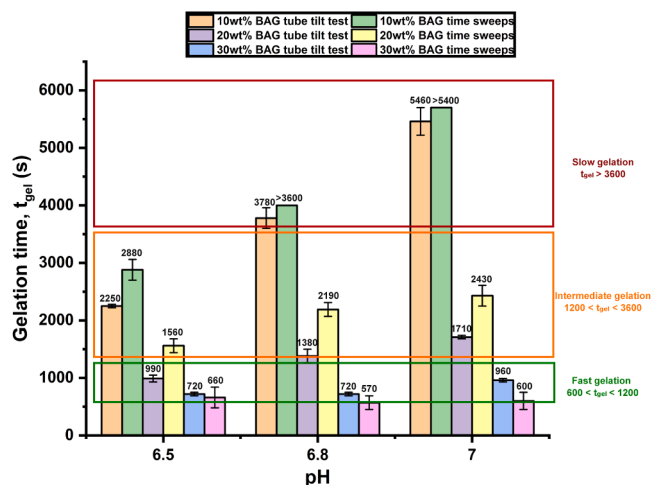


Fig. 4. Gelation time, (t_{gel}) for samples with 10, 20, and 30 wt% BAG at initial pH levels 6.5, 6.8, and 7.0, measured by tube tilt test and time sweep. The gelation process was differentiated into zones of fast, intermediate, and slow gelation. At each time point $n = 3$ and values are given as average \pm standard deviation.

elastic character, typical of a gel-like structure. Notably, the $\tan \delta$ values (G''/G') were generally below 0.1, suggesting an elastic (solid-like) response and well-crosslinked network in most samples [31].

In contrast, the 20 wt% BAG samples at pH 6.8, and 10 wt% BAG samples at pH 7.0 exhibited $\tan \delta$ values exceeding 0.1. This suggests a shift toward more viscous (fluid-like) behavior and indicating less effective crosslinking. Additionally, all 30 wt% BAG samples maintained $\tan \delta$ values between 0.072 and 0.078, demonstrating a stable network structure with effective crosslinking. This data shows that higher BAG loading leads to a stronger and more elastic network, while variations in pH affects viscoelasticity.

4. Discussion

The novelty of this work lies in real-time monitoring of both pH and temperature during the ionic crosslinking of polysaccharide hydrogels – an aspect rarely explored in past research. Existing studies have primarily focused on post-gelation analysis or the effects of crosslinking density at wider pH changes, which are also critical for biomaterials design. Furthermore, pH changes we monitored were in the very narrow range close to neutral (from 6.5 to 7.0).

In our previous work, we observed that the gelation time of GG/BAG composites decreased with increasing glass loading [18]. At 55 °C and initial pH 6.5, gelation time measured by the tube tilt test, ranged from

Table 2

Viscoelastic properties of GG/BAG composites at various pH levels and BAG loadings. Values of storage modulus (G') and loss modulus (G'') were obtained within the LVER at a frequency of 0.4 Hz. For each condition, $n = 3$; values are reported as mean \pm standard deviation.

BAG, [wt%]	$pH = 6.5$			$pH = 6.8$			$pH = 7.0$		
Amplitude sweep									
	LVER, [%]	G'/G'' Crossover point, [%]		LVER, [%]	G'/G'' Crossover point, [%]		LVER, [%]	G'/G'' Crossover point, [%]	
10	0.01 – 0.10	1.71		0.01 – 0.10	2.62		0.01 – 0.10	2.77	
20	0.01 – 0.16	2.83		0.01 – 0.25	2.85		0.01 – 0.25	2.88	
30	0.01 – 0.25	4.56		0.01 – 0.40	4.56		0.01 – 0.40	4.64	
Frequency sweep									
	G' , [Pa]	G'' , [Pa]	Tan δ	G' , [Pa]	G'' , [Pa]	Tan δ	G' , [Pa]	G'' , [Pa]	Tan δ
10	907 \pm 210	84 \pm 31	0.092	1051 \pm 105	86 \pm 21	0.082	1369 \pm 213	148 \pm 79	0.108
20	2575 \pm 978	188 \pm 83	0.073	2695 \pm 312	435 \pm 160	0.161	2617 \pm 358	170 \pm 65	0.065
30	1819 \pm 646	132 \pm 61	0.072	1780 \pm 149	136 \pm 22	0.076	2737 \pm 847	213 \pm 67	0.078

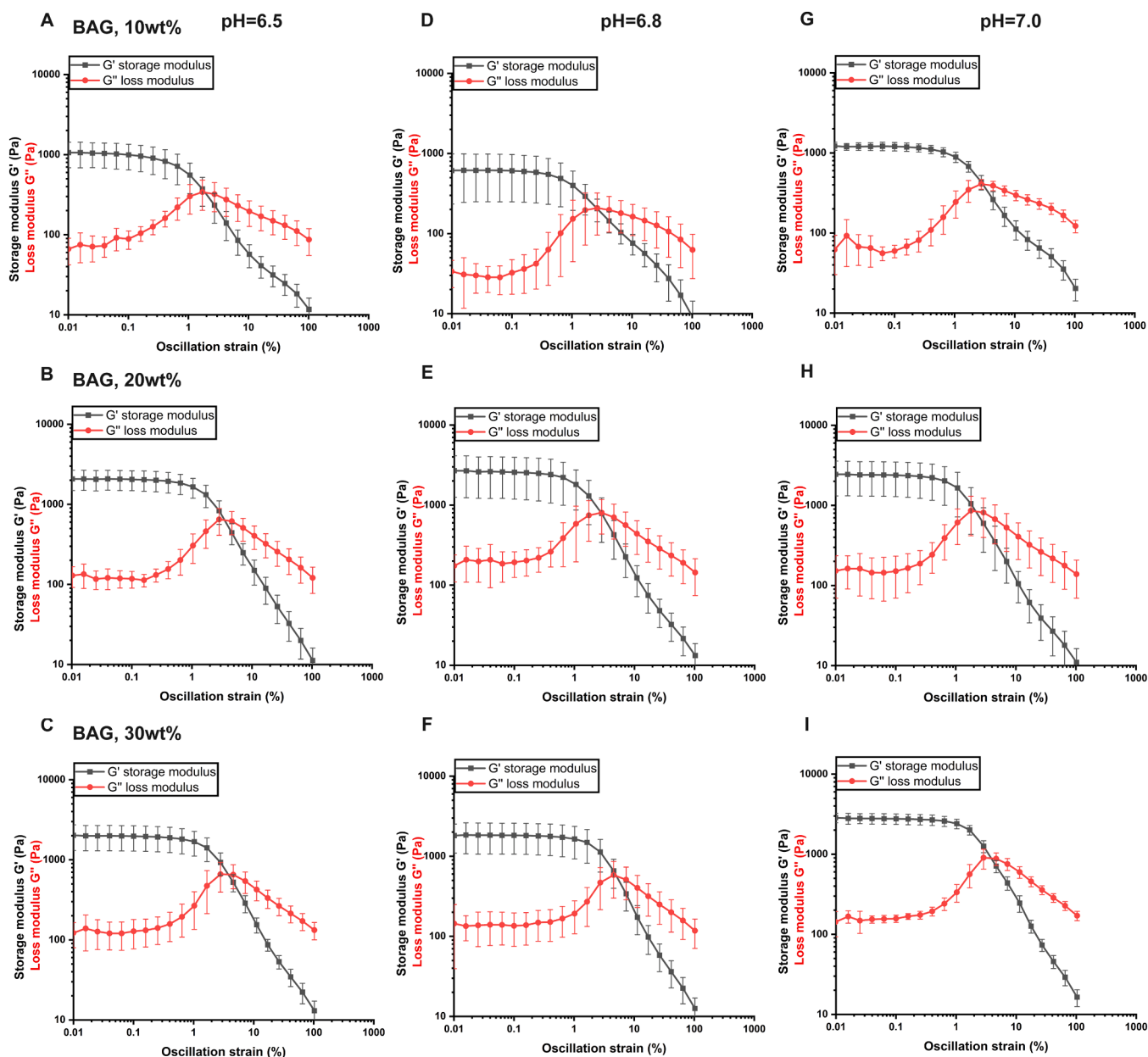


Fig. 5. Amplitude sweeps at various pH and glass loadings: pH 6.5 (left column): A) 10 wt% BAG, B) 20 wt% BAG, C) 30 wt% BAG; pH 6.8 (central column): D) 10 wt% BAG, E) 20 wt% BAG, F) 30 wt% BAG; pH 7.0 (right column): G) 10 wt% BAG, H) 20 wt% BAG, I) 30 wt% BAG. At each time point $n = 3$ and values are given as average \pm standard deviation.

5 min (10 wt% BAG) to 2.5 min (30 wt% BAG). In the current study, conducted at 23 °C, gelation time for identical samples ranged from 37.5 to 12 min, demonstrating a similar trend: higher BAG loading accelerates gelation [15]. This acceleration is attributed to the increased number of crosslinking ions, which promotes the formation of a denser crosslinked network. Gelation times of 10–60 min are usually desired in biomedical applications to allow sufficient time for pipetting, injecting, or even 3D printing [32,33]

GG undergoes a coil-helix transition when heated between 30 °C – 50 °C, followed by helix aggregation during cooling, forming a physical gel network [15,34]. Real-time monitoring of pH and temperature during the preparation and gelation phases revealed key insights into the crosslinking kinetics (Table 1, Table S1). BAG addition increased the temperature from the initial 23 °C (T_1) by 5 °C – 14 °C (T_2), depending on BAG loading and initial pH (Table 1). This rise is likely due to ultrasonic energy absorption and heat generation from rapid particle

movement, which appeared capable of activating the double-helix formation [35]. Temperature then dropped by 7 °C – 13 °C (T_3), reflecting the stabilization of sonication-induced heating, but rose again slightly by 1 °C – 5 °C (T_5), possibly due to exothermic double-helix formation or residual crosslinking heat [15,36].

During preparation and gelation stages, pH gradually increased, with higher BAG loading (30 wt%) causing greater pH shifts. At 30 wt% BAG, pH increased to 7.32 – 7.50 (pH_5), compared to 7.06 – 7.22 at 10 wt% BAG, suggesting enhanced ion release (Table 1).

Alvarez-Lorenzo *et al.* discussed how the ionization state of carboxylic groups (-COOH) regulates crosslinking and drug release behaviors in ionic polysaccharide gels [37]. At higher pH (7.40), deprotonation to -COO⁻ increases electrostatic repulsion, swelling, and drug release. At lower pH (1.30), protonation reduces repulsion and swelling due to stronger hydrogen bonding [31,37]. Our study extends this understanding by showing that even small changes in initial pH (6.5, 6.8, 7.0)

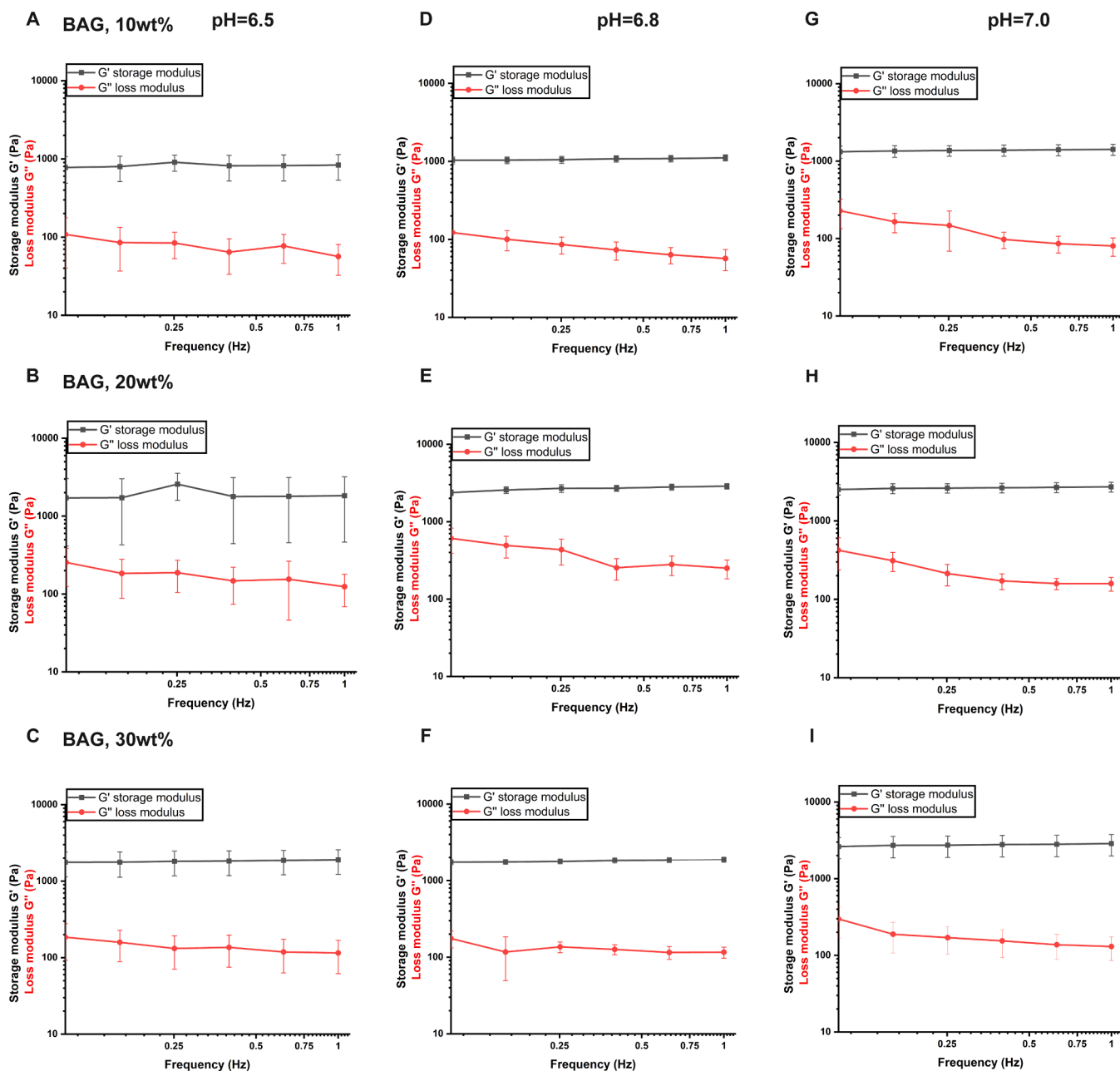


Fig. 6. Frequency sweeps at various pH and glass loadings. pH 6.5 (left column): A) 10 wt% BAG, B) 20 wt% BAG, C) 30 wt% BAG; pH 6.8 (central column): D) 10 wt% BAG, E) 20 wt% BAG, F) 30 wt% BAG; pH 7.0 (right column): G) 10 wt% BAG, H) 20 wt% BAG, I) 30 wt% BAG. At each time point $n = 3$ and values are given as average \pm standard deviation.

and BAG content (10, 20, 30 wt%) significantly influence gelation time. For instance, at 10 wt% BAG, gelation time increased from 2800 s (approximately 46 min) at pH 6.5 to more than 5400 s (90 min) at pH 7.0. At 20 wt%, it rose from 1560 to 2430 s (26 min to 40.5 min) (Fig. 7). This result suggests that near-neutral pH reduces available crosslinking sites, thereby slowing down the gelation, already with very small pH changes.

These findings align with previous work of Picone *et al.*, who demonstrated that increasing pH reduced the enthalpy of the coil-helix transition in deacylated GG, thus lowering the energy barrier for gelation [38]. Similar pH -dependent effects have been observed in other polysaccharide hydrogels like xanthan gum and guar gum. In carboxymethylated guar and xanthan gums, low pH (1.3) conditions yield denser crosslinking and slower drug release, while higher pH (7.4) increases the ionization, swelling and release rates [37]. Cationic guar

gums behave oppositely, forming stronger interactions at low pH and weakening at higher pH .

Our previous theoretical modeling showed that at 10 wt% BAG, there were 314 potential crosslinks but only 77 available crosslinking cations - indicating an ion deficit. At 20 wt%, there were 279 potential crosslinks and 141 cations, still insufficient. Only at 30 wt% BAG, 346 divalent ions exceed 244 potential crosslinks, enabling faster gelation [18]. This supports earlier findings by Lau *et al.*, who showed that GG/Ca^{2+} ratios strongly affect gelation time, with Ca^{2+} levels modulating gelation temperature and speed [39].

Rheological analysis via amplitude and frequency sweeps revealed that increasing BAG loading expanded the LVER, indicating enhanced elasticity. At higher pH , LVER expansion was more evident in samples with 20–30 wt% BAG, while 10 wt% BAG remained unaffected. The G'/G'' crossover point also shifted slightly with increasing pH and more

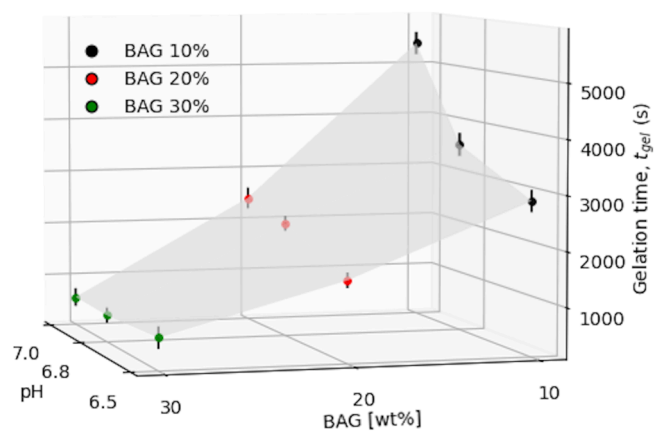


Fig. 7. A 3D surface plot illustration of pH and glass loading's effect on gelation time (t_{gel}) in GG/BAG samples: the mean values of gelation time (t_{gel}) from time sweep measurements are shown with colored dots standard deviations are shown with black error bars. The light gray surface is added to help reading the plot to visualize the co-dependent effect of both pH and glass loading on the t_{gel} .

significantly with higher BAG content, as expected [4]. G' and G'' also increased with pH , peaking at 20 wt% BAG, indicating optimal crosslinking-to-ion ratio for stable gel formation.

While Gering *et al.* examined GG rheology through chemical modifications (e.g. oxidation, sodium substitution, chain scission), our study focuses on ionic crosslinking via BAG, showing its strong influence on gel elasticity and mechanical tuning [7]. In their work, time sweep rheology was employed to monitor the gelation kinetics of GG formulations crosslinked with Ca^{2+} and spermidine bioamine under low strain and frequency. All formulations formed self-supporting hydrogels within 30 min. In contrast, in our study, where GG was crosslinked with BAG, gelation times varied significantly—from as short as 9 min to over 90 min—depending on the glass loading.

Cassanelli's work found that GG gels prepared under acidic conditions (pH 3.5) had greater mechanical strength and Young's modulus than those at pH 7, highlighting the role of pH in gel integrity [40]. Besiri, studying alginate gelation kinetics, found that enhanced crosslinker diffusion through microchannels accelerated gelation and improved mechanical properties [41]. Unlike Cassanelli's and Besiri's studies, our work focuses on how BAG incorporation within small pH changes (6.5–7.0) reduces pH sensitivity and enhances gel stability under physiologically relevant conditions.

Tanaka *et al.* modeled gelation kinetics based using theoretical reaction parameters such as concentration, temperature, and functionality [8]. In contrast, we determined gelation time experimentally from the plateau region of the G' curve (Fig. 3). Our data shows that even modest increase in pH from 6.5 to 7.0 reduces available crosslinking sites and delays gelation. Similarly, Yamamoto *et al.* found faster gelation of GG gels at lower pH (2.0–4.0) and elevated temperatures (70–90 °C) [42].

Finally, we implemented a case study on a single polysaccharide to investigate the impact of changes in pH and crosslinker concentrations on gelation time. However, similar research on structure-property relationships based on modifications of those parameters could be conducted for other polysaccharides. This would contribute to a generalized understanding of chemical interactions in polysaccharide-based composite hydrogels.

5. Conclusions

The results demonstrated that crosslinking occurred faster at more acidic pH and higher glass loading. Gelation in GG/BAG crosslinking was monitored through real-time pH and temperature changes. Ultrasonication caused initial heating enough to trigger the coil-helix transition, followed by cooling, then a final temperature rise from viscosity

changes or exothermic GG helix formation. A slight pH increase (6.5–7.0) prolonged gelation time at 20 wt% BAG, but had no significant effect at 30 wt%, as the higher ion release dominated the gelation process over the effect of initial pH . Increased BAG loading led to enhanced stiffness and elasticity, as expected, and was evidenced by low $\tan \delta$ and high G' and G'' . By establishing a matrix of easily modifiable process parameters, this study supports the potential use of GG/BAG composites in 3D printing, injectability for implant devices, and other applications requiring specific rheological properties.

Abbreviations

BAG, borosilicate bioactive glass, 13–93B20; GG, gellan gum; G , storage modulus; G' , loss modulus; HEPES, (4-(2-hydroxyethyl)-1-piperazineethanesulfonic acid); LVER, linear viscoelastic region; t_{gel} , gelation time; mix, mixing; wt%, weight percentage;

Funding

The authors acknowledge the Academy of Finland (# 353173) and the Centre of Excellence in Body-on-Chip Research (CoEBoC) for financial support and for raw materials of gellan gum and consumables. The authors would like to thank the Academy of Finland (project # 331924) for raw materials for glasses, and consumables. Janne T. Koivisto would like to thank Tampere Institute for Advanced Studies for the financial support.

CRediT authorship contribution statement

Koivisto Janne Tapio: Writing – review & editing, Validation, Supervision, Project administration, Methodology, Formal analysis, Conceptualization. **Minna Kellomäki:** Writing – review & editing, Supervision, Resources, Project administration, Funding acquisition, Conceptualization. **Jonathan Massera:** Writing – review & editing, Supervision, Resources, Project administration, Conceptualization. **Anastasiia Astanina:** Writing – original draft, Visualization, Validation, Investigation, Formal analysis, Data curation, Conceptualization.

Declaration of Competing Interest

The authors declare the following financial interests/personal relationships which may be considered as potential competing interests: Minna Kellomäki reports financial support was provided by Research Council of Finland. Jonathan Massera reports financial support was provided by Research Council of Finland. If there are other authors, they declare that they have no known competing financial interests or personal relationships that could have appeared to influence the work reported in this paper.

Acknowledgments

The Authors would like to thank B.Sc. Savvas Giannettou and B.Sc. Abdul Rehman for their help in conducting real-time pH and temperature measurements during the gelation of GG/BAG composites. Additionally, authors would like to thank Dr. Kyriacos Yiannacou for overall support. Some of the unpublished results were presented at the 2024 Young Ceramists Additive Manufacturing Forum (yCAM 2024).

Appendix A. Supporting information

Supplementary data associated with this article can be found in the online version at [doi:10.1016/j.mtcomm.2025.114133](https://doi.org/10.1016/j.mtcomm.2025.114133).

Data availability

Data will be made available on request.

References

- [1] D. Dörr, U. Kuhn, V. Altstädt, Rheological study of gelation and crosslinking in chemical modified polyamide 12 using a multiwave technique, *Polymers* 12 (2020) 855, <https://doi.org/10.3390/polym12040855>.
- [2] E. Jain, L. Hill, E. Canning, S.A. Sell, S.P. Zusiak, Control of gelation, degradation and physical properties of polyethylene glycol hydrogels through the chemical and physical identity of the crosslinker, *J. Mater. Chem. B* 5 (2017) 2679–2691, <https://doi.org/10.1039/c6tb0350e>.
- [3] A.V. Shibaev, D.A. Muravlev, A.K. Muravleva, V.V. Matveev, A.E. Chalykh, O. E. Philippova, pH-dependent gelation of a stiffanionic polysaccharide in the presence of metal ions, *Polymers* 12 (2020) 868, <https://doi.org/10.3390/polym12040868>.
- [4] G. Stojkov, Z. Niyazov, F. Picchioni, R.K. Bose, Relationship between structure and rheology of hydrogels for various applications, *Gels* 7 (2021) 255, <https://doi.org/10.3390/gels7040255>.
- [5] B.P.M. Duarte, M.J. Moura, Using rheological monitoring to determine the gelation kinetics of chitosan-based systems, *Math. Biosci. Eng.* 20 (2023) 1176–1194, <https://doi.org/10.3934/mbe.2023054>.
- [6] R. Sun Han Chang, J.C.W. Lee, S. Pedron, B.A.C. Harley, S.A. Rogers, Rheological analysis of the gelation kinetics of an enzyme cross-linked PEG hydrogel, *Biomacromolecules* 20 (2019) 2198–2206, <https://doi.org/10.1021/acs.biomac.9b00116>.
- [7] C. Gering, A. Rasheed, J.T. Koivisto, J. Párraga, S. Tuukkanen, M. Kellomäki, Chemical modification strategies for viscosity-dependent processing of gellan gum, *Carbohydr. Polym.* 269 (2021) 118335, <https://doi.org/10.1016/j.carbpol.2021.118335>.
- [8] F. Tanaka, Gelation time of network-forming polymer solutions with reversible cross-link junctions of variable multiplicity, *Gels* 9 (2023) 379, <https://doi.org/10.3390/gels9050379>.
- [9] L.R. Stevens, K.J. Gilmore, G.G. Wallace, M. In het Panhuis, Tissue engineering with gellan gum, *Biomater. Sci.* 4 (2016) 1276–1290, <https://doi.org/10.1039/c6bm00322b>.
- [10] K. Vuornos, M. Ojansivu, J.T. Koivisto, H. Hakkanen, B. Belay, T. Montonen, H. Huhtala, M. Kaarlainen, L. Hupa, M. Kellomäki, J. Hyttinen, J.A. Ihalainen, S. Miettinen, Bioactive glass ions induce efficient osteogenic differentiation of human adipose stem cells encapsulated in gellan gum and collagen type I hydrogels, *Mater. Sci. Eng. C* 99 (2019) 905–918, <https://doi.org/10.1016/j.msec.2019.02.035>.
- [11] J.T. Koivisto, T. Joki, J.E. Parraga, R. Paakkonen, L. Ylä-Outinen, L. Salonen, I. Jonkkari, M. Peltola, T.O. Ihalainen, S. Narkilahti, M. Kellomäki, Bioamine-crosslinked gellan gum hydrogel for neural tissue engineering, *Biomed. Mater.* 12 (2017) 025014, <https://doi.org/10.1088/1748-605X/aa62b0>.
- [12] E. Miyoshi, T. Takaya, K. Nishinari, Effects of salts on the gel-sol transition of gellan gum by differential scanning calorimetry and thermal scanning rheology, *Thermochim. Acta* 267 (1995) 269–287, [https://doi.org/10.1016/0040-6031\(95\)02485-9](https://doi.org/10.1016/0040-6031(95)02485-9).
- [13] P. Vincchi, S.U. Rawal, M.M. Patel, Biodegradable hydrogels, in E. Chappel (Ed.), *Developments in Biomedical Engineering and Bioelectronics, Drug Delivery Devices and Therapeutic Systems*, Academic Press, 2021, pp. 395–419.
- [14] P. Gadziński, A. Froelich, B. Jadač, M. Wojtylko, A. Tatarek, A. Bialek, J. Kryzstofiak, M. Gackowski, F. Otto, T. Osmałek, Ionotropic gelation and chemical crosslinking as methods for fabrication of modified-release gellan gum-based drug delivery systems, *Pharmaceutics* 15 (2023) 108, <https://doi.org/10.3390/pharmaceutics15010108>.
- [15] E.R. Morris, K. Nishinari, M. Rinaudo, Gelation of gellan - a review, *Food Hydrocoll.* 28 (2012) 373–411, <https://doi.org/10.1016/j.foodhyd.2012.01.004>.
- [16] H. Jongprasitkul, S. Turunen, V.S. Parihar, M. Kellomäki, Two-step crosslinking to enhance the printability of methacrylated gellan gum biomaterial ink for extrusion-based 3D bioprinting, *Bioprinting* 25 (2022) e00185, <https://doi.org/10.1016/j.bprint.2021.e00185>.
- [17] T.E.L. Douglas, W. Piwowarczyk, E. Pamula, J. Liskova, D. Schaubroeck, S.C. G. Leeuwenburgh, G. Brackman, L. Balcaen, R. Detsch, H. Declercq, K. Cholewa-Kowalska, A. Dokupil, V.M.J.I. Cuijpers, F. Vanhaecke, R. Cornelissen, T. Coenye, A.R. Boccaccini, P. Dubruel, Injectable self-gelling composites for bone tissue engineering based on gellan gum hydrogel enriched with different bioglasses, *Biomed. Mater.* 9 (2014) 045014, <https://doi.org/10.1088/1748-6041/9/4/045014>.
- [18] A. Astanina, J.T. Koivisto, M. Hannula, T. Salminen, M. Kellomäki, J. Massera, Chemical interactions in composites of gellan gum and bioactive glass: self-crosslinking and in vitro dissolution, *Front. Chem.* 11 (2023) 1133374, <https://doi.org/10.3389/fchem.2023.1133374>.
- [19] L.L. Hench, The story of bioglass, *J. Mater. Sci. Mater. Med.* 17 (2006) 967–978, <https://doi.org/10.1007/s10856-006-0432-z>.
- [20] R.M. Day, A.R. Boccaccini, S. Shurey, J.A. Roether, A. Forbes, L.L. Hench, S. M. Gabe, Assessment of polyglycolic acid mesh and bioactive glass for soft-tissue engineering scaffolds, *Biomaterials* 25 (2004) 5857–5866, <https://doi.org/10.1016/j.biomaterials.2004.01.043>.
- [21] A. Szczodra, A. Houaoui, T. Salminen, M. Hannula, V.A. Gobbo, S. Ghanavati, S. Miettinen, J. Massera, Pore graded borosilicate bioactive glass scaffolds: in vitro dissolution and cytocompatibility, *J. Mater. Sci. Mater. Med.* 35 (2024) 06791, <https://doi.org/10.1007/s10856-024-06791-1>.
- [22] A. Szczodra, A. Houaoui, R. Agniel, L. Sicard, S. Miettinen, J. Massera, C. Gorin, Boron substitution in silicate bioactive glass scaffolds to enhance bone differentiation and regeneration, *Acta Biomater.* 186 (2024) 489–506, <https://doi.org/10.1016/j.actbio.2024.07.053>.
- [23] A. Houaoui, I. Lyyra, R. Agniel, E. Pauthe, J. Massera, M. Boissiere, Dissolution, bioactivity and osteogenic properties of composites based on polymer and silicate or borosilicate bioactive glass, *Mater. Sci. Eng. C* 107 (2020) 110340, <https://doi.org/10.1016/j.msec.2019.110340>.
- [24] M. Ojansivu, A. Mishra, S. Vanhatupa, M. Juntunen, A. Larionova, J. Massera, S. Miettinen, The effect of S53P4-based borosilicate glasses and glass dissolution products on the osteogenic commitment of human adipose stem cells, *PLOS One* 13 (2018) e0202740, <https://doi.org/10.1371/journal.pone.0202740>.
- [25] E. Zeimaran, S. Pourshahrestani, A. Fathi, N. Anuar bin Abd Razak, N. Adib Kadri, A. Sheikhi, F. Baimo, Advances in bioactive glass-containing injectable hydrogel biomaterials for tissue regeneration, *Acta Biomater.* 136 (2021) 1–36, <https://doi.org/10.1016/j.actbio.2021.09.034>.
- [26] F. Zhang, X. Wang, N. Guo, H. Dai, Y. Wang, Y. Sun, G. Zhu, Influence of different pH values on gels produced from tea polyphenols and low acyl gellan gum, *Gels* 9 (2023) 368, <https://doi.org/10.3390/gels9050368>.
- [27] A. Houaoui, A. Szczodra, M. Lallukka, L. El-Guermah, R. Agniel, E. Pauthe, J. Massera, M. Boissiere, New generation of hybrid materials based on gelatin and bioactive glass particles for bone tissue regeneration, *Biomolecules* 11 (2021) 444, <https://doi.org/10.3390/biom11030444>.
- [28] M. Siekkinen, O. Karlström, L. Hupa, Dissolution of bioactive glass S53P4 in a three-reactor cascade in continuous flow conditions, *Open Ceram.* 13 (2023) 100327, <https://doi.org/10.1016/j.oceram.2022.100327>.
- [29] W.E. Rochefort, S. Middleman, Rheology of xanthan gum: salt, temperature, and strain effects in oscillatory and steady shear experiments, *J. Rheol.* 31 (1987) 337–369, <https://doi.org/10.1122/1.549953>.
- [30] K. Hyun, S.H. Kim, K.H. Ahn, S.J. Lee, Large amplitude oscillatory shear as a way to classify the complex fluids, *J. NonNewton. Fluid Mech.* 107 (2002) 51–65, [https://doi.org/10.1016/S0377-0257\(02\)00141-6](https://doi.org/10.1016/S0377-0257(02)00141-6).
- [31] C.N.R. Amaral, P.F. Oliveira, L.G. Pedroni, C.R.E. Mansur, Viscoelastic behavior of hydrogel-based xanthan gum/aluminum lactate with potential applicability for conformance control, *J. Appl. Polym. Sci.* 138 (2021) 50640, <https://doi.org/10.1002/app.50640>.
- [32] C.J. Maxwell, A.M. Soltisz, W.W. Rich, A. Choi, M.A. Reilly, K.E. Swindle-Reilly, Tunable alginate hydrogels as injectable drug delivery vehicles for optic neuropathy, *J. Biomed. Mater. Res. A* 110 (2022) 1621–1635, <https://doi.org/10.1002/jbm.a.37412>.
- [33] H.-H. Roh, H.-S. Kim, C. Kim, K.-Y. Lee, 3D printing of polysaccharide-based self-healing hydrogel reinforced with alginate for secondary cross-linking, *Biomedicines* 9 (2021) 1224, <https://doi.org/10.3390/biomedicines9091224>.
- [34] I. Giavasis, L.M. Harvey, B. McNeil, Gellan gum, *Crit. Rev. Biotechnol.* 20 (2000) 177–211, <https://doi.org/10.1080/07388550008984169>.
- [35] G. Sellani, D. Fernandes D, A. Nahari, M.F. de Oliveira, C. Valois, W.C. Pereira, C. B. Machado, Assessing heating distribution by therapeutic ultrasound on bone phantoms and *in vitro* human samples using infrared thermography, *J. Ther. Ultrasound* 4 (2016) 13, <https://doi.org/10.1186/s40349-016-0058-7>.
- [36] S. Tanaka, K. Nishinari, Unassociated molecular chains in physically crosslinked gellan gels, *Polym. J.* 39 (2007) 397–403, <https://doi.org/10.1295/polymj.PJ2006149>.
- [37] C. Alvarez-Lorenzo, B. Blanco-Fernandez, A.M. Puga, A. Concheiro, Crosslinked ionic polysaccharides for stimuli-sensitive drug delivery, *Adv. Drug Deliv. Rev.* 65 (2013) 1148–1171, <https://doi.org/10.1016/j.addr.2013.04.016>.
- [38] C.S.F. Picone, R.L. Cunha, Influence of pH on formation and properties of gellan gels, *Carbohydr. Polym.* 84 (2011) 662–668, <https://doi.org/10.1016/j.carbpol.2010.12.045>.
- [39] M.H. Lau, J. Tang, A.T. Paulson, Effect of polymer ratio and calcium concentration on gelation properties of gellan/gelatin mixed gels, *Food Res. Int.* 34 (2001) 879–886, [https://doi.org/10.1016/S0963-9969\(01\)00112-0](https://doi.org/10.1016/S0963-9969(01)00112-0).
- [40] M. Cassanelli, V. Prosapio, I. Norton, T. Mills, Acidified/basified gellan gum gels: the role of the structure in drying/rehydration mechanisms, *Food Hydrocoll.* 82 (2018) 346–354, <https://doi.org/10.1016/j.foodhyd.2018.04.024>.
- [41] I.N. Besiri, T.B. Goudoulas, E. Fattahi, T. Becker, In situ evaluation of alginate-Ca²⁺ gelation kinetics, *J. Appl. Polym. Sci.* 140 (2023) e54252, <https://doi.org/10.1002/app.54252>.
- [42] F. Yamamoto, R.L. Cunha, Acid gelation of gellan: effect of final pH and heat treatment conditions, *Carbohydr. Polym.* 68 (2007) 517–527, <https://doi.org/10.1016/j.carbpol.2006.11.009>.